Learning from Topology:
Cosmological Parameter Estimation from the Large-scale Structure

Jacky H. T. Yip [*1] **Adam Rouhiainen** [*1] **Gary Shiu** [1]

Abstract

The topology of the large-scale structure of the universe contains valuable information on the underlying cosmological parameters. While persistent homology can extract this topological information, the optimal method for parameter estimation from this tool remains an open question. To address this, we propose a neural network model to map persistence images to cosmological parameters. Through a parameter recovery test, we demonstrate that our model makes accurate and precise estimates, considerably outperforming Bayesian inference approaches.

1. Introduction

The recent decade has brought the field of cosmology powerful machine learning tools to analyze the vast amount of data from large-scale sky surveys. In this paper, we propose a new method to attack the long-standing problem of cosmological parameter estimation from the large-scale structure of the universe. It has been shown that decent results can be achieved using deep learning (e.g., Ravanbakhsh et al., 2017; Ntampaka et al., 2020; Wen et al., 2023; Hwang et al., 2023). However, despite their effectiveness, neural networks trained directly on low-level data (such as dark matter fields and galaxy maps) lack interpretability and provide little understanding of the underlying physics due to the high degrees of freedom in the input data.

Simply put, cosmologists seek summary statistics that not only stem from physical intuitions but also retain a substantial amount of information. In this regard, we consider applying persistent homology (PH) to point clouds of dark matter halos. PH is a topological data analysis tool that quantifies the robustness of topological features across length

[*]Equal contribution [1]Department of Physics, University of Wisconsin-Madison, Madison, WI 53706, USA. Correspondence to: Jacky H. T. Yip <hyip2@wisc.edu>.

scales, allowing for a natural description of the multi-scale patterns in the large-scale structure that the halos trace. Recent studies have demonstrated that this tool can be used to detect primordial non-Gaussianity (Biagetti et al., 2021), identify cosmic structures (Xu et al., 2019), and differentiate dark matter models (Cisewski-Kehe et al., 2022).

The raw outputs of a PH computation are persistence diagrams, which can be conveniently vectorized as persistence images. We may flatten and use them directly for Bayesian inference by assuming a Gaussian likelihood via a covariance structure between pixels (e.g., Cole & Shiu, 2018). However, such a high-dimensional covariance matrix often behaves poorly and requires a considerable amount of additional data for its estimation. More critically, the covariance does not capture higher-order correlations, such as patterns spanned by multiple neighbouring pixels.

We propose to train a convolutional neural network (CNN) model on persistence images to estimate the underlying cosmological parameters. For comparisons, we perform the same task by Bayesian inference using two summary statistics: a histogram-based statistic also derived from PH, and the power spectrum. The former has been recently studied in the literature, while the latter is a baseline statistic ubiquitous in the cosmological community. We find that our CNN model recovers parameters much more accurately and precisely, thus improving on the conventional approaches. This work also serves as a pioneering example of integrating computational topology and machine learning in the context of cosmology.

2. Cosmology and the Large-scale Structure

The ΛCDM model is by far the best-supported theory of our universe (Dodelson & Schmidt, 2020). In particular, it explains the evolution of inhomogeneities in the matter distribution in an expanding spacetime. This paper focuses on two parameters within this model: the matter density Ω_{m}, and the clustering amplitude σ_8. While the impacts of these parameters on the evolution are well understood in the linear regime, beyond which we generally resort to N-body simulations. Hence, the inverse problem, i.e., parameter estimation from the late-time matter distribution,

holds significance both in theory and in practice.

The Zel'dovich approximation, a non-linear model of the evolution of non-interacting particles, predicts that ellipsoidal distributions of matter collapse along their axes into clusters, filaments, and walls (Zel'dovich, 1970; Hidding et al., 2013). These components assemble hierarchically to form multi-scale halo clusters, filament loops, and cosmic voids, which are the topological features we track with PH.

3. Persistence Statistics

3.1. Persistent Homology

We apply PH to 3D point clouds of dark matter halos. A point cloud is first triangulated as a simplicial complex, i.e., a set of points, line segments, triangles, and tetrahedrons. We can then define a *parametrized* family of nested subcomplices called a filtration. That is, as the filtration parameter ν grows, simplices are added to the subcomplex according to a specified set of rules. We use the αDTMℓ-filtration (Biagetti et al., 2021; Chazal et al., 2017) in this work. The idea is roughly that ν is taken as a length scale, and a simplex is added if its "size" is smaller than ν.
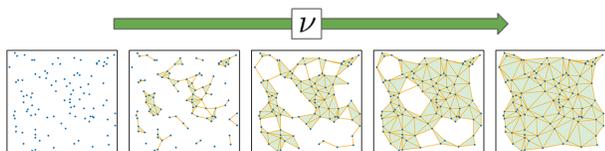

Figure 1. Example of a filtration on a 2D point cloud. The simplicial subcomplex evolves with the filtration parameter ν. Topological features (islands and loops) are created and subsequently trivialized in the process.

For every value of ν, we identify topological features in the corresponding subcomplex. They are the 0-, 1-, and 2-cycles, which represent islands, closed loops, and enclosed cavities, respectively. Physically, they correspond to halo clusters, filament loops, and cosmic voids in the large-scale structure. Hence, the evolution of the simplicial subcomplex throughout the filtration can be characterized by a set of $(\nu_{\text{birth}}, \nu_{\text{death}})$ values at which n-cycles are born and killed.

3.2. From Persistence Diagrams to Summary Statistics

The list of $(\nu_{\text{birth}}, \nu_{\text{death}})$ pairs can be recast in the $(\nu_{\text{birth}}, \nu_{\text{persist}} = \nu_{\text{death}} - \nu_{\text{birth}})$ coordinates. For each of the three n values, we can plot $(\nu_{\text{birth}}, \nu_{\text{persist}})$ of all the once-existed n-cycles. These three plots called the persistence diagrams are the raw outputs of the PH computation. We can further convert them into useful data vectors:

Persistence Images - We assign a Gaussian kernel to each point in a persistence diagram. Then we discretize the birth-

persistence plane and sum up all the kernel contributions within each pixel to obtain a 2D array of numbers, called a persistence image (Adams et al., 2017).

Histograms - Following Biagetti et al., 2022 and Yip et al., 2023, we construct histograms from the distributions of ν_{birth} and ν_{persist} for all n. The $3 \times 2 = 6$ histograms are then concatenated into a 1D array of numbers.

4. The Power Spectrum

The halo auto power spectrum $P^{\text{hh}}(k)$ measures the contribution to the density contrast (the difference between the local and mean densities divided by the mean density) of the halo field from modes of wavenumber k. It quantifies the "lumpiness" of the halo distribution as a function of scale. As a summary statistic, the power spectrum has been well-understood (Peebles, 1980) and used widely to access the cosmological information in the halo field (e.g., Coulton et al., 2023; Gabriel Jung & et al, 2023). Hence, it is included in our analysis as a baseline for comparison against the persistence statistics.

We use persistence images for our CNN model (**PI-CNN**), and the histograms and power spectrum for Bayesian inference (**Hist-BI** and **PS-BI**).

5. Simulation and Dataset

This section details all the computational steps (Figure 2) we take to create our dataset of summary statistics.

5.1. Dark Matter Simulation

We employ FLOWPM (Modi et al., 2021) to produce snapshots of late-time distributions of dark matter particles. Although it lacks exact dynamics, this fast solver is sufficiently accurate for this work as a proof of concept (see Feng et al., 2016 for discussions on accuracy issues).

Given cosmological parameter values, we can compute the primordial matter power spectrum, from which Gaussian random fields at a required redshift can be generated via the transfer function (Eisenstein & Hu, 1998) and linear growth factors. We begin evolving the Gaussian field at $z = 9$ for numerical stability, and a total of 10 time-steps are used. Snapshots are taken at redshift $z = 0.5$ to match standard survey samples (e.g., the BOSS CMASS galaxies, Reid et al., 2016) for the convenience of future analyses on galaxy maps. Each simulation box is $(256\,h^{-1}\text{Mpc})^3$ in volume and contains $(160)^3$ particles, resulting in a particle resolution on par with state-of-the-art simulations such as the QUIJOTE suite (Villaescusa-Navarro et al., 2020).

For both the training of our CNN model and likelihood evaluation, we vary Ω_{m} and σ_8 in our simulations, where

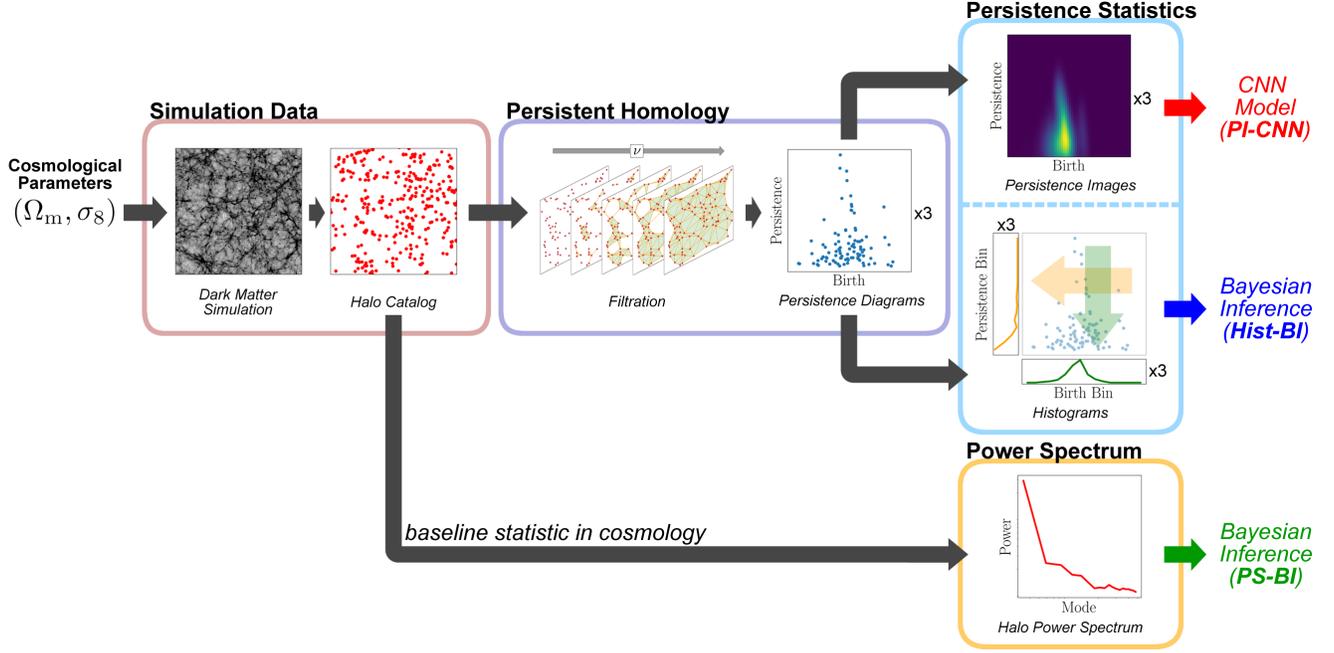*Figure 2.* Given a $(\Omega_{\mathrm{m}}, \sigma_8)$ pair, we generate a realization of the dark matter field at $z = 0.5$ in a $(256\,h^{-1}\mathrm{Mpc})^3$ box. We locate the halos in the field and apply persistent homology to the halo catalog. The output from the filtration is a list of $(\nu_{\mathrm{birth}}, \nu_{\mathrm{persist}})$ values, plotted as persistence diagrams. We can 1) pixelate the diagrams into persistence images for our CNN model, or 2) sum up the topological features along each axis into histograms for Bayesian inference. "$\times 3$" refers to having three copies for the 0-, 1-, and 2-cycles. The halo auto power spectrum, also for Bayesian inference, is measured directly from the halo catalog and provides a baseline result for comparison against the persistence statistics.

$\Omega_{\mathrm{m}} \in [0.21, 0.41]$ and $\sigma_8 \in [0.72, 0.92]$. Each range is divided into 60 equal intervals for a total of 3600 distinct $(\Omega_{\mathrm{m}}, \sigma_8)$ configurations, and we generate 10 independent realizations for each configuration. Hence, there is a grand total of 36000 simulations in the main dataset. We use the Planck 2015 results for all other cosmological parameters (final column of Table 4 in Planck Collaboration, 2016). Moreover, a flat universe is assumed such that we take the dark energy density as $\Omega_\Lambda = 1 - \Omega_{\mathrm{m}}$ whenever applicable.

We further produce 15000 realizations at the fiducial cosmology $(\Omega_{\mathrm{m}}, \sigma_8) = (0.3089, 0.8159)$. We use 5000 of these to estimate the covariance matrix in the likelihood and the remaining 10000 for the parameter recovery test.

5.2. Halo Catalog

We use the ROCKSTAR halo finder (Behroozi et al., 2013) to identify dark matter halos in each simulation snapshot. We set the force resolution to $0.005\,h^{-1}\mathrm{Mpc}$ and keep other settings as default. In each fiducial box, $\sim$2000 halos are identified, which is comparable to QUIJOTE as a credibility check. Hence, each halo catalog is a list of halo positions in real space to which we apply PH.

5.3. Summary Statistics

Our PH code relies on the GUDHI libraray (The GUDHI Project, 2015). From persistence diagrams to images, we employ SCIKIT-LEARN (Pedregosa et al., 2011) to fit the Gaussian kernel density model, with the bandwidth parameter set to 2. Each point in the diagrams is also customarily weighted by $\sqrt{\nu_{\mathrm{persist}}}$ to emphasize more persistent features. The dimensions of each persistence image is 64^2. For the histograms, we use the same binnings across all parameter configurations. After concatenation, we further downsample the full histogram statistic to $6 \times 16 = 96$ numbers for optimal inference accuracy.

We use PYLIANS (Villaescusa-Navarro, 2018) to compute the halo auto power spectrum. There is only the monopole since the halos are in real space. The power spectrum is truncated by imposing $k_{\max} = 0.4\,h\mathrm{Mpc}^{-1}$, for the reason that our halo catalogs from the fast simulations might not be very reliable in the highly non-linear regime (we have checked that the inference results are similar for $k_{\max} = 0.3$, 0.4, and $0.5\,h\mathrm{Mpc}^{-1}$, thus our conclusion does not depend on this choice). We also model the shot noise as Poisson distributed and subtract $1/n_{\mathrm{h}}$ from the power spectrum, where n_{h} is the catalog's halo number density. However, in the estimation of the covariance matrix, the shot noise is

retained for it contributes as a source of uncertainty.

6. Estimation Methods

6.1. Convolutional Neural Network Model

We design a neural network model that combines in parallel a CNN with a stack of dense layers to map the persistence images to $(\Omega_{\mathrm{m}}, \sigma_8)$. The inputs to the model are the 0-, 1-, and 2-cycle persistence images stacked into 3 channels, and the outputs are 2 numbers for our 2 parameters (Figure 3).

On the CNN side of our parallel networks, we use four sequential blocks, each made of a 3×3 convolution with no padding, and ReLU activation functions. Each convolution is followed by a 2×2 max pooling layer with stride 2. After the fourth block, the data is reduced to 2×2 pixels, and two dense layers with ReLUs follow to output 2 numbers.

On the dense side, we turn the persistence images into a 1D list of data by summing along the birth and persistence axes of the image. As this summed data is only $3 \times 2 \times 64 = 384$ numbers, we use a stack of dense layers on the entire data without pooling. We tested different combinations of 1D convolutions and pooling, with and without ResNet blocks, and found no increase in model performance over simply using a stack of 5 dense layers with ReLUs.

We find a modest increase in model precision (1σ's are reduced by $\sim 10\%$) with the parallel networks over just the CNN side alone. The 2 numbers output from each side of the model are finally averaged into our $(\Omega_{\mathrm{m}}, \sigma_8)$ estimate.

We use 33000 persistence images for our training set and 3000 for the validation set. For every $(\Omega_{\mathrm{m}}, \sigma_8)$ configuration, we average 10 corresponding images pixelwise. While this averaging does reduce the number of training set images by a factor of 10, we find increased precision of our model even with the extra risk of overfitting. Our loss function is the mean squared error between the model output parameters and true parameter values. By analyzing training and validation performance, we have carefully chosen the number of parameters in our network (detailed in Figure 3) to maximize performance while preventing overfitting. The model has 1.34 million parameters in total. To additionally help prevent overfitting, we use a small batch size of 16. We train with a learning rate of 10^{-4} with the Adam optimizer, decreased by a factor of 0.75 when the loss plateaus.

A potential hurdle we suspect in using a traditional CNN on persistence images is the overall smoothness of each image. In a traditional image classification dataset, we encounter, e.g., many distinct edges in each image; the convolutional filters in the first few layers of the network would learn to detect these edges. It may require a more novel approach to capture more of the features of persistence images.
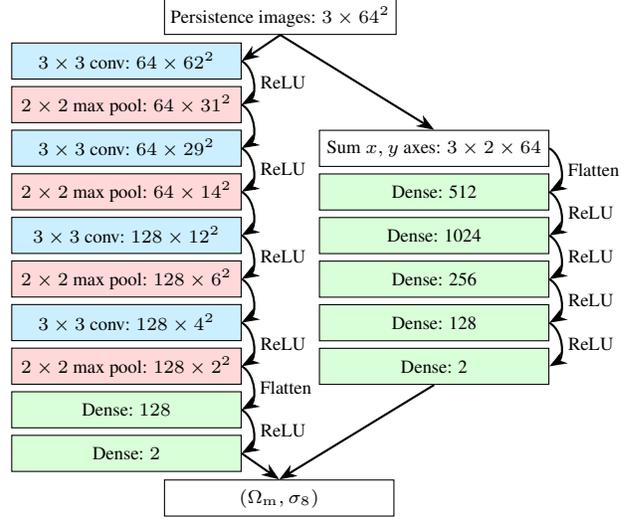

Figure 3. Architecture of our CNN model, with layer names and output dimensions.

6.2. Bayesian Inference

We adopt a flat prior $p(\boldsymbol{\theta})$ and a Gaussian likelihood $\mathcal{L}(\boldsymbol{\theta}|\boldsymbol{D})$ such that we have for the log-posterior:

$$\ln p(\boldsymbol{\theta}|\boldsymbol{D}) = -\frac{1}{2}(\boldsymbol{D} - \boldsymbol{\mu}(\boldsymbol{\theta}))^T C^{-1} (\boldsymbol{D} - \boldsymbol{\mu}(\boldsymbol{\theta})) + \text{const.}$$

by Bayes' theorem. Here $\boldsymbol{\theta}$ is one of the 3600 $(\Omega_{\mathrm{m}}, \sigma_8)$ configurations at which the log-posterior is to be numerically evaluated. $\boldsymbol{\mu}(\boldsymbol{\theta})$ is the data vector of the full histogram statistic or power spectrum, measured at $\boldsymbol{\theta}$ and averaged over 10 realizations. $\boldsymbol{D}$ is an observation, also averaged over 10 realizations, measured at some unknown configuration that we want to recover. C is the covariance matrix, and we include the Hartlap factor (Eq. (17) in Hartlap et al., 2006) for the unbiased estimation of C^{-1}. The constant term $\text{const.} = \ln \frac{p(\boldsymbol{\theta})}{p(\boldsymbol{D})}$ can be ignored as it plays no role in finding the maximum a posteriori (MAP) estimate.

It is worth noting that the likelihood function of the histogram statistic can be checked empirically to be Gaussian (Biagetti et al., 2022; Yip et al., 2023). For the power spectrum, assuming a Gaussian likelihood is customary (Carron, 2013). Moreover, with the averaging over realizations (such that the central limit theorem applies), the Gaussian likelihood for inference is well-motivated overall.

We use a 2D Gaussian filter to smooth out the noise in the numerically evaluated log-posterior, with σ of the kernel set to 1 and 0.2 pixels (optimized for inference accuracy) for the histogram statistic and power spectrum respectively. The MAP estimate is taken to be the $(\Omega_{\mathrm{m}}, \sigma_8)$ configuration that maximizes the (log-)posterior.
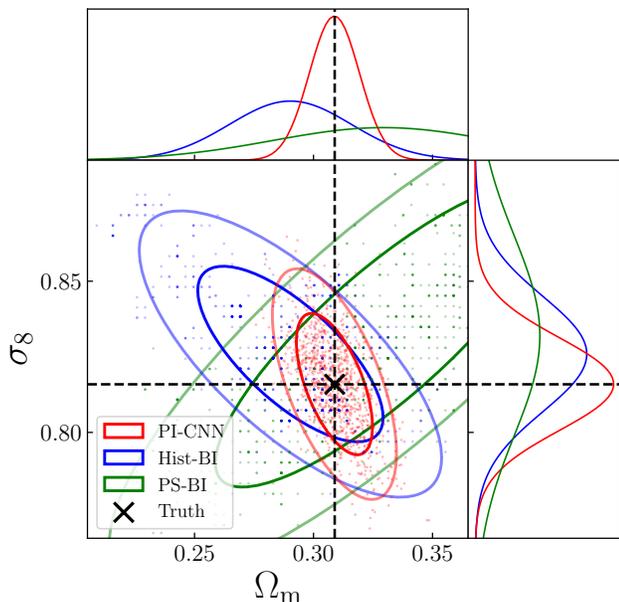
Figure 4. Red, blue, and green dots in the central panel mark the 1000 $(\Omega_\mathrm{m}, \sigma_8)$ values estimated on the fiducial measurements by the CNN model and Bayesian inference approaches. We fit a Gaussian to each distribution, and the contours mark the 68% and 95% confidence intervals. Side panels show the marginalized Gaussians. The true values are located by the crosshairs.

7. Parameter Recovery Test

We conduct a parameter recovery test to compare the PI-CNN, Hist-BI, and PS-BI pipelines. All statistics are averaged over every 10 boxes in the test dataset of 10000 fiducial boxes, i.e., we have 1000 independent observations at $(\Omega_\mathrm{m}, \sigma_8) = (0.3089, 0.8159)$. This averaging is in accordance with how the estimation methods are trained, as described in the previous section.

We present our result in Figure 4. In the central panel, we plot the PI-CNN estimates in red, Hist-BI in blue, and PS-BI in green. The MAP estimates are restricted to grid points because the log-posterior is evaluated on the discretized Ω_m-σ_8 plane. We fit a bivariate Gaussian to each of the distributions and plot the contours for the 68% and 95% confidence interval. The marginalized Gaussians are plotted in the side panels. The mean estimates are $(0.3088 \pm 0.0105, 0.8160 \pm 0.0154)$ for PI-CNN, $(0.2903 \pm 0.0256, 0.8259 \pm 0.0191)$ for Hist-BI, and $(0.3294 \pm 0.0464, 0.8320 \pm 0.0329)$ for PS-BI. The true fiducial values are marked by the crosshairs.

Comparing between the PH-based methods, the PI-CNN Gaussian is accurately centered on the true value while that for Hist-BI is fairly biased. The variance in the PI-CNN estimates is also lower, particularly for Ω_m. Both Gaussians show that there is a negative correlation between the two

parameters, which is a common result for many summary statistics (e.g., mass function of low-redshift galaxy clusters, Vikhlinin et al., 2009). Intriguingly, the Pearson correlation coefficient for PI-CNN (-0.60) is less negative than that for Hist-BI (-0.72). This implies that the 2D persistence images contain extra information extractable by the CNN model for breaking partially the parameter degeneracy.

The PS-BI result is the most biased and has much higher variance. This is not surprising because the power spectrum is a two-point statistic, while PH theoretically probes higher-order correlations by tracking topological features each constructed from typically many points (though it arguably misses some long-range information). Interested readers may refer to Yip et al., 2023 for a comprehensive analysis on the cosmological information content from PH compared with the two- and three-point statistics.

8. Conclusion and Outlook

We have put cosmology, computational topology, and machine learning together by training a CNN model on persistence images for cosmological parameter estimation. From the parameter recovery test, we have found that the CNN model makes accurate and precise estimates, outperforming Bayesian inference methods that use a histogram-based persistence statistic and the power spectrum, respectively. It has also been observed that persistence statistics outperform the power spectrum regardless of the estimation method, implying that PH easily extracts more cosmological information than the two-point statistic.

Two immediate directions are as follows: First, we should use galaxy maps and take into account observational effects, such as sky cuts and instrumental systematics, to make our model readily applicable to survey data. Second, the effectiveness of our CNN model can be investigated by, e.g., studying the saliency maps (Simonyan et al., 2013), which may help us gain insight into the information content of persistence images relevant to cosmology.

Broader Impact

In this work we use machine learning to learn cosmological information from the topology of simulated dark matter halo catalogs. This research benefits the theoretical cosmology community by demonstrating that a machine learning method of analyzing topological information can outperform traditional methods. Considering the result of this work, some previous works on persistent homology in cosmology that did not use a machine learning approach might be revisited, and we encourage future works to consider using machine learning. The data used in this work are taken from cosmological simulations, and we use well-known machine learning and statistical techniques, so we see no

ethical or societal consequences introduced by this work.

References

Adams, H., Emerson, T., Kirby, M., and et al. Persistence images: A stable vector representation of persistent homology. *The Journal of Machine Learning Research*, 18, 2017.

Behroozi, P. S., Wechsler, R. H., and Wu, H.-Y. The rockstar phase-space temporal halo finder and the velocity offsets of cluster cores. *The Astrophysical Journal*, 762(109), 2013.

Biagetti, M., Cole, A., and Shiu, G. The persistence of large scale structures i: Primordial non-gaussianity. *Journal of Cosmology and Astroparticle Physics*, 04(061), 2021.

Biagetti, M., Calles, J., Castiblanco, L., and et al. Fisher forecasts for primordial non-gaussianity from persistent homology. *Journal of Cosmology and Astroparticle Physics*, 10(002), 2022.

Carron, J. On the assumption of gaussianity for cosmological two-point statistics and parameter dependent covariance matrices. *Astronomy and Astrophysics*, 551(A88), 2013.

Center for High Throughput Computing. Center for high throughput computing, 2006. URL https://chtc.cs.wisc.edu/.

Chazal, F., Fasy, B., Lecci, F., and et al. Robust topological inference: distance to a measure and kernel distance. *The Journal of Machine Learning Research*, 18, 2017.

Cisewski-Kehe, J., Fasy, B. T., Hellwing, W., and et al. Differentiating small-scale subhalo distributions in cdm and wdm models using persistent homology. *Physical Review D*, 106, 2022.

Cole, A. and Shiu, G. Persistent homology and non-gaussianity. *Journal of Cosmology and Astroparticle Physics*, 03(025), 2018.

Coulton, W. R., Villaescusa-Navarro, F., Jamieson, D., Baldi, M., and et al. Quijote-png: The information content of the halo power spectrum and bispectrum. *The Astrophysical Journal*, 943(2), 2023.

Dodelson, S. and Schmidt, F. (eds.). *Modern Cosmology*. Academic Press, 2020.

Eisenstein, D. J. and Hu, W. Baryonic features in the matter transfer function. *The Astrophysical Journal*, 496:605–614, 1998.

Feng, Y., Chu, M.-Y., Seljak, U., and McDonald, P. Fastpm: a new scheme for fast simulations of dark matter and haloes. *Monthly Notices of the Royal Astronomical Society*, 463:2273–2286, 2016.

Gabriel Jung, Dionysios Karagiannis, M. L. M. B. and et al. Quijote-png: Quasi-maximum likelihood estimation of primordial non-gaussianity in the nonlinear halo density field. *The Astrophysical Journal*, 948(2), 2023.

Hartlap, J., Simon, P., and Schneider, P. Why your model parameter confidences might be too optimistic. unbiased estimation of the inverse covariance matrix. *Astronomy and Astrophysics*, 464(1), 2006.

Hidding, J., Shandarin, S. F., and van de Weygaert, R. The zel'dovich approximation: key to understanding cosmic web complexity. *Monthly Notices of the Royal Astronomical Society*, 437, 2013.

Hwang, S. Y., Sabiu, C. G., Park, I., and Hong, S. E. The universe is worth 64^3 pixels: Convolution neural network and vision transformers for cosmology. 2023.

Modi, C., Lanusse, F., and Seljak, U. Flowpm: Distributed tensorflow implementation of the fastpm cosmological n-body solver. *Astronomy and Computing*, 37(100505), 2021.

Ntampaka, M., Eisenstein, D. J., Yuan, S., and Garrison, L. H. A hybrid deep learning approach to cosmological constraints from galaxy redshift surveys. *The American Astronomical Society*, 889(151), 2020.

Pedregosa, F., Varoquaux, G., Gramfort, A., Michel, V., Thirion, B., Grisel, O., Blondel, M., Prettenhofer, P., Weiss, R., Dubourg, V., Vanderplas, J., Passos, A., Cournapeau, D., Brucher, M., Perrot, M., and Duchesnay, E. Scikit-learn: Machine learning in Python. *Journal of Machine Learning Research*, 12:2825–2830, 2011.

Peebles, P. J. E. (ed.). *The large-scale structure of the universe*. Princeton University Press, 1980.

Planck Collaboration. Planck 2015 results. xiii. cosmological parameters. *Astronomy & Astrophysics*, 594(A13), 2016.

Ravanbakhsh, S., Oliva, J., Fromenteau, S., and et al. Estimating cosmological parameters from the dark matter distribution. 2017.

Reid, B., Ho, S., Padmanabhan, N., and et al. Sdss-iii baryon oscillation spectroscopic survey data release 12: galaxy target selection and large-scale structure catalogues. *Monthly Notices of the Royal Astronomical Society*, 455:1553–1573, 2016.

Simonyan, K., Vedaldi, A., and Zisserman, A. Deep inside convolutional networks: Visualising image classification models and saliency maps. 2013.

The GUDHI Project. *GUDHI User and Reference Manual*. GUDHI Editorial Board, 2015.

Vikhlinin, A., Kravtsov, A. V., Burenin, R. A., and et al. Chandra cluster cosmology project iii: Cosmological parameter constraints. *The Astrophysical Journal*, 692, 2009.

Villaescusa-Navarro, F. Pylians: Python libraries for the analysis of numerical simulations. Astrophysics Source Code Library, record ascl:1811.008, 2018.

Villaescusa-Navarro, F., Hahn, C., Massara, E., and et al. The quijote simulations. *The Astrophysical Journal Supplement*, 250(2), 2020.

Wen, Y., Yu, W., and Li, D. Cosnas: Enhancing estimation on cosmological parameters via neural architecture search. *New Astronomy*, 99(101955), 2023.

Xu, X., Cisewski-Kehe, J., Green, S., and Nagai, D. Finding cosmic voids and filament loops using topological data analysis. *Astronomy and Computing*, 27, 2019.

Yip, J. H. T., Biagetti, M., Cole, A., and et al. Constraining cosmology with persistent homology: Cosmological parameters and primordial non-gaussianity. *To appear*, 2023.

Zel'dovich, Y. B. Gravitational instability: An approximate theory for large density perturbations. *Astronomy and Astrophysics*, 5, 1970.